MINERALOGY OF THE VALLES MARINERIS FROM TES AND THEMIS. F. S. Anderson[1], V.E. Hamilton[1], and P.R. Christensen[2], [1]University of Hawai'i at Manoa, Hawai'i Institute of Geophysics and Planetology, 1680 East-West Road, POST 526B, Honolulu, HI 96822 (anderson@higp.hawaii.edu), [2]Dept. Geological Sciences
ASU, Box 876305, Tempe, AZ 85287-6305, (phil.christensen@asu.edu).

Introduction:

This study uses Mars Global Surveyor Thermal Emission Spectrometer (TES) and 2001 Mars Odyssey Thermal Emission Imaging System (THEMIS) data to examine the mineralogy of the wall and floor deposits of the Valles Marineris (VM), where exposed. We present results from TES analysis of the VM region as well as detailed analysis of Melas Chasma, and note a remarkable degree of correlation between high-resolution THEMIS thermal images and full resolution TES data. Using THEMIS as a mapping tool, we will correlate the observed TES and THEMIS spectra, identifying unique local compositional signatures, complementing previous studies that averaged data at a regional scale [0]. The observed composition and stratigraphic relationships determined from the Mars Orbiting Laser Altimeter (MOLA) can then be used to constrain the processes acting on the walls and floors of the VM.

Background:

Valles Marineris: The VM form a series of linear subparallel troughs that vary in width from 20 to 600 km, with average depths of 6-7 km [1-3]. Two competing interpretations have developed for the formation of VM: (1) tectonic subsidence, or (2) fluvial or subsurface withdrawal [4-12,2]. The recent discovery of subsurface channels just north and east of VM [13] provides new insight into where the water within the troughs may have gone. The VM have been characterized as having significant layered deposits, a wide variety of morphologies, and numerous regions with low albedo surfaces. Understanding the mineralogy of these features would allow us to address a range of genetic hypotheses for these features, including, for example:

- Is the layering observed in the walls and on the floors of the VM igneous or sedimentary (**Figure 1**)?
- Are the interior layered deposits volcanic or lacustrine (REFS)?
- Are there extensive basal basalt layers?
- What are the blocky deposits observed at the 2003 MER Melas landing site (not selected), and how did they form (**Figure 1**)?
- Is there compositional evidence for water?

Wall rock is exposed on the sloping walls of bounding the troughs of the VM. Between 4 and 8

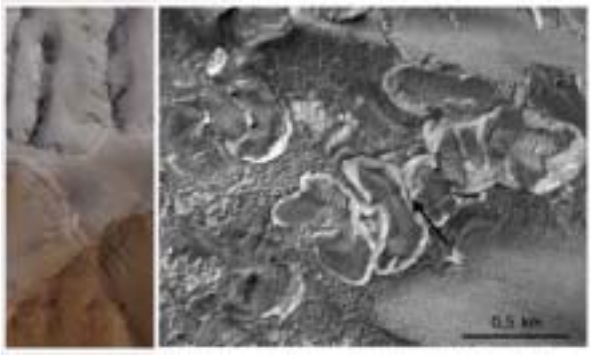

Figure 1: Layers revealed in MOC narrow angle imaging are thought to be igneous (right). Unique and poorly understood structure of the blocky deposits found in Melas Chasma make them a high priority mineralogy target.

layers in the top kilometer of the canyons have been recognized in Viking data [2], while MOC has revealed that local bedrock exposures are common and contain extensive layering [14,15] that have been interpreted to be composed of volcanic strata [16-18,2].

Additional deposits on the floor of the troughs include landslide and aeolian deposits. Landslides are observed at a variety of scales in all of the major trough systems [2], and have IRTM & TES inertias consistent with rough blocky surfaces likely to ideal targets for THEMIS and TES analysis. The avalanches appear consistent with dry rock in non-lacustrine environments, though some evidence for an ice component ice is suggested by a channel leading from one of the landslide aprons [2]. Aeolian deposits are comprised of dark dunes that are sometimes obscured by dust infall [19,20].

The interior layered deposits observed in the VM appear to be composed of alternating light and dark beds of approximately 70 m thickness. Despite first being imaged in Mariner 9 images [21], their origin remains enigmatic. Proposed hypotheses for the genesis of the ILD's of the VM must consider the probable effects of both extension and fluvial processes related to the formation of the troughs. Hypotheses for the formation of ILDs focus include sedimentary deposits formed in lakes [21-25] or volcanic deposits [26-31], though other discounted possibilities exist [2]. Recently, it has been suggested that the alternating light dark layering seen in the interior deposit suggests a sedimentary origin for the deposits [25].

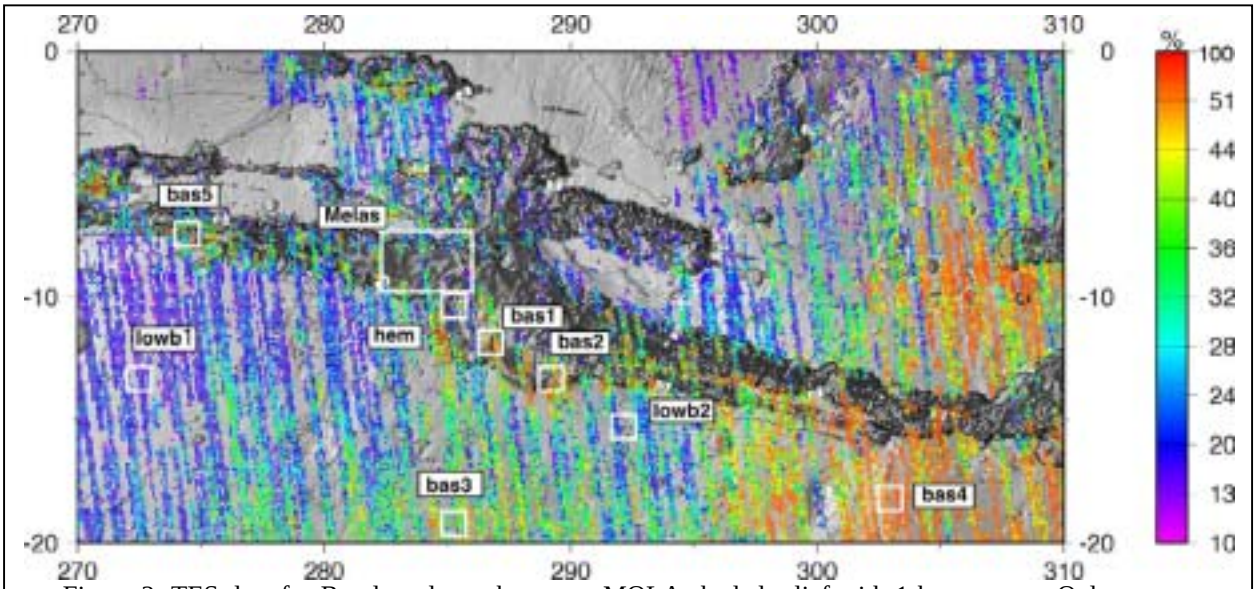

Figure 2: TES data for Basalt end member, over MOLA shaded relief with 1 km contour. Only concentrations exceeding the ~10% detection limit [7] and [4] are plotted. Note that the lower elevations of the eastern VM are highly basaltic, as are the southern walls and central troughs in Coprates, Melas, Ius, Noctis, potions of Candor, and Hebes Chasma. Regions with high albedo are left blank.

***TES & THEMIS*:** TES is currently acquiring thermal infrared (5 – 50 µm) spectra of the Martian surface at spatial resolutions of approximately 3 x 6 km per pixel and spectral resolutions of 5-10 wavenumbers [32]. THEMIS is acquiring spectra of the surface from 6.78-14.88 µm, in ten bands, and has a spatial resolution of 100 m/pixel. Spectral absorptions in Martian mid-IR data are attributable to atmospheric CO_2 and dust, water-ice clouds, and surface materials. *Smith et al.* [33] and *Bandfield et al.* [34-35] have demonstrated that the spectral signatures of the atmospheric components may be removed via radiative transfer modeling, and to first order, by linear deconvolution. The surface spectrum that remains after atmospheric removal is indicative of several properties of the surface materials including bulk composition, relative abundances of minerals, and particle size. The easiest surface spectra to interpret are those obtained in low-albedo, high thermal inertia regions that are dominated by coarse (10's – 100's of µm) sands, regolith, and/or bedrock with little dust.

It is important to note that the slopes of the canyon walls in the VM can be steep (up to 34°) causing TES & THEMIS to observe sloped surfaces. Slopes may become a problem in regions where steeply dipping walls meet near-horizontal surfaces (e.g., at the bottom of a canyon wall), which could create spectral complications due to the complex interaction of the radiated energy from the two surfaces [*P. Christensen*, personal communication, 2000]. The MOLA data used for this study were derived from the 128 pixel/degree digital elevation model. TES and THEMIS data were collocated with MOLA data gridded to TES resolution.

In general, the TES data were constrained by avoiding bad orbit flags, orbits beyond 7000 (after which spacecraft vibration influenced the spectra), data with temperatures < 260K, or albedo > 0.24. The data were further decimated by removing end member estimates >120% (caused by processing errors) or with spectral RMS misfits > 0.015 (to provide tight constraints on results; median misfit in the VM data is 0.05). To minimize masking of the surface, we further constrained the data by requiring dust concentrations to be < 0.15. Dust and ice, as previously reported, demonstrate an inverse correlation, while the basaltic andesite end member is influenced by overlap with a band with a dust band [*J. L. Bandfield*, pers. comm., 2003], thus, this study focuses on the basaltic and hematite end members.

Method & Results:

Regional Basalt Signature: First we made compositional maps of the end member deconvolutions of the TES dataset that are performed with each downlink from MGS. These maps were then plotted on images of the topography of the VM (**Figure 2**). The predicted end members are based on the deconvolution method of *Smith et al.* [33] and *Bandfield et al.* [34] that atmospherically correct all incoming TES spectra using seven atmospheric and surface end members (two dust, two water-ice cloud, basalt, basaltic andesite, and hematite). These seven spectra are not representative of every possible surface, and may map some regions with only moderate success [*J. L. Bandfield*, pers. comm., 2003].

The map of basalt displays two levels of end member concentration; one generally >30%, the other generally <24%. These materials likely represent aeolian or dust draping, or a mineralogic change with no stratigraphic relationship. The high concentration of basalt is also spatially associated with the Hesperian ridged plains (*Hr*), Noachian subdued craters (Npl_2), and ridged units (*Nplr*) [35], and may be consistent with low viscosity volcanism identified for *Hr*. Lastly, the superposed younger plains of Syria, Solis, and Sinai are associated with andesitic compositions. Our observations of hematite in the VM are similar to those seen by *Christensen et al.*, [37].

Individual groups of 6-30 spectra from the high and low basalt regions (**Figure 3**) were deconvolved and mineralogy determined from them (**Figure 4**). The mineralogy was constrained to consist of 52 end-members, including: Atmospheric (4), Pyroxenes (11), Feldspars (10), Olivines (6), Oxides (3), Phyllosilicates (9), A.mphiboles (3), Salts (4), Glass, and Quartz end-members. After normalizing for blackbody and atmosphere, the detection limit is 15-25%. The high and low basalt compositions have been shown to be statistically different using cluster analysis, and the high basalt appears different from the global basalt endmember; low basalt regions appear similar to the global andesite endmember.

Melas Chasma: Next we studied the Melas Chasma region in detail (**Figure 5**), to determine compositional differences between interior layered deposits, blocky deposits, landslides, and undifferentiated aeolian bedforms. The results from this effort (**Figure 6**), though preliminary, show that the spectra are statistically seperable, and different from the global basalt and andesite end-members, commonly being reduced in feldspar, phyllosilicates, and glass, while demonstrating olivine enrichment. The two interior layered deposits (ILD and ILM) appear different, with the ILM unit appearing to be mantled by the aeolian bedform unit. In general, the landslide values are variable in composition from landslide to landslide, perhaps reflecting variance in the dust cover on these units.

Correlation of TES & THEMIS: We have closely studied the high basalt deposits derived from TES associated with the southern rim of the VM near central Melas, and have observed that these units correlate with THEMIS thermal and albedo contrasts (**Figure 7**). We will show a complete decorelation stretch of this region (**Figure 8**) at the conference.

We have also examined locales in which TES indicated a hematite abundance > 25%, and observed that these TES pixels are often associated with low-lying layered outcrops on the floor of Melas.

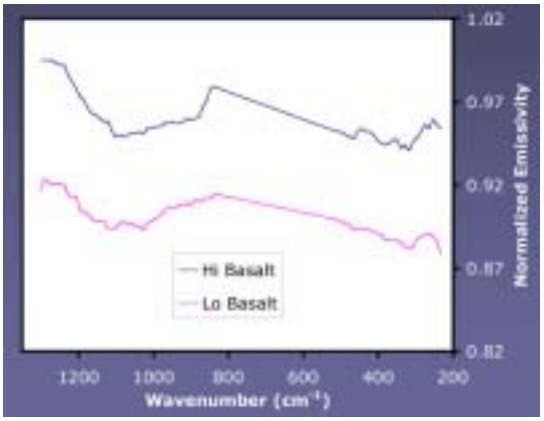

Figure 3: Average spectra for high and low basalt regions.

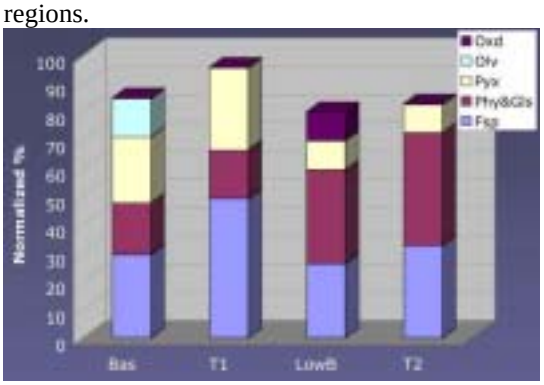

Figure 4: Composition from spectra in Fig. 3.

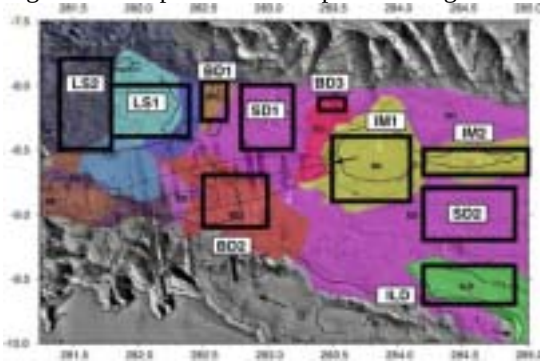

Figure 5: Locations of analysis in Melas

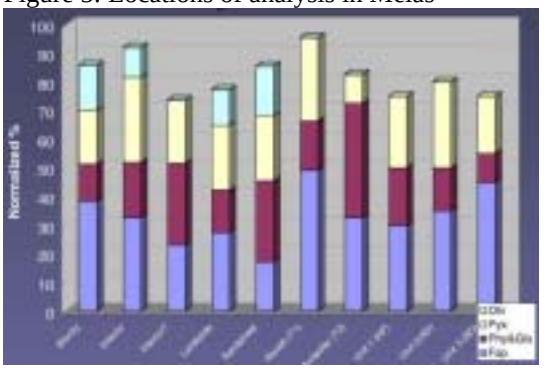

Figure 6: Compositions from Fig. 5.

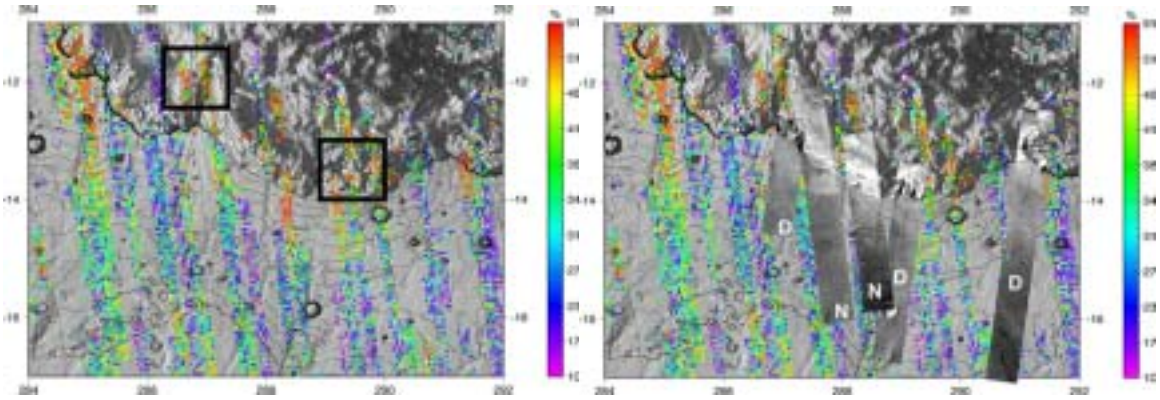

Figure 7: Association of individual high basalt TES pixels with thermo-physically warmer regions on the southern rim of central Melas Chasma.

Conclusion:

Our initial results indicate that there is no evidence in the basaltic units for more aqueous alteration products than is observed for global surface types. In the future, we will add CO_2, water vapor, and surface dust end-members [Bandfield & Smith, 2003]. As our results may be influenced by regional averaging, we will deconvolve individual icks and detectors & make high resolution maps, provide statistical analysis of compositional results, and correlate results with MOLA topography, slopes, & roughness. Lastly, we will continue to expand our analysis to include THEMIS datasets.

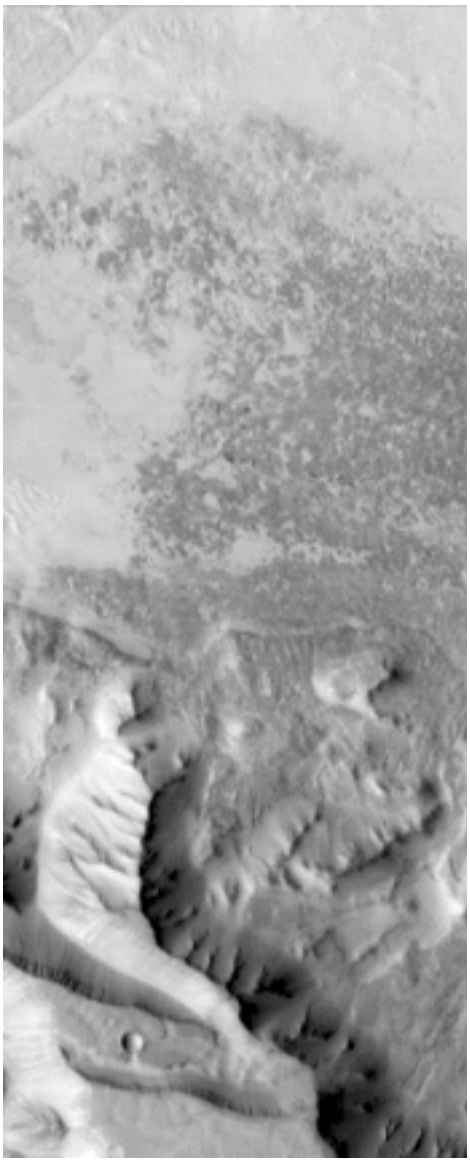

Figure 8: Blocky deposits in Melas.

References:

[0] Bandfield et al., *Science*, *287*, 1626-1630, 2000. [1] *Schultz and Frey*, 1989. [2] *Lucchitta et al*., 1992. [3] *Peulvast and Masson*, 1993b. [4] *Schultz*, 1990. [5] *Schultz*, 1991. [6] *Schultz*, 1995. [7] *Schultz*, 1997. [8] *Tanaka*, 1997. [9] *Mege and Masson*; 1996a. [10] *Mege and Masson*; 1996b. [11] *Peulvast and Masson*, 1993a. [12] *Peulvast and Masson*, 1993b. [13] *Zuber et al*., 2000. [14] *Malin et al.*, 1998. [15] *McEwen et al.*, 1999. [16] *Scott and Carr*, 1978; [17] *Greeley and Spudis*, 1981; [18] *Scott and Tanaka*, 1986; [19] *Thomas*, 1982; [20] *Lucchitta*, 1990. [21] *McCauley*, 1978. [22] *Nedell et al*., 1987; [23] *Komatsu et al.*, 1993 [24] *Weitz and Parker*, 2000; [25] *Malin and Edgett*, 2000 [26] *Peterson*, 1981; [27] *Lucchitta*, 1990; [28] *Lucchitta et al*., 1994; [29] *Weitz*, 1999; [30] *Chapman and Tanaka*, 2000; [31] *Chapman and Lucchitta*, 2000, [32] Christensen et al., *J. Geophys. Res.*, *97*, 7719-7734, 1992. [33] Smith et al., *J. Geophys. Res.*, *105*, 9589-9607, 2000. [34] Bandfield et al., *J. Geophys. Res.*, *105*, 9573-9587, 2000. [35] Scott and Tanaka, USGS, Geologic map of Mars, *M 15M 0/90 G*, Flagstaff, Ariz.,1986. [36] Christensen et al., *J. Geophys. Res.*, 2002. [37] *Christensen et al., J. Geophys. Res.*, *105*, 9609-9621, [2000a].